Application of Vector Spherical Harmonics to the Magnetisation of Mars' Crust

David Gubbins[1,2], Yi Jiang[2], Simon E. Williams[3], Keke Zhang[2]

[1]School of Earth and Environment, University of Leeds, UK
[2]State Key Laboratory of Lunar and Planetary Science, Macau University of Science and Technology, Macau
[3]State Key Laboratory of Continental Dynamics, Department of Geology, Northwest University, Xi'an, China

Key Points:

- Vector spherical harmonic analysis can help with exploration of magnetic stuctures in Mars' crust
- Absence of magnetic field at satellite altitude does not necessarily mean the crust beneath has been demagnetised
- Absence of anomalies at large impact craters implies weak shallow magnetisation elsewhere

Corresponding author: D. Gubbins, gubbins@earth.leeds.ac.uk

Abstract

Mars has a magnetic field originating in its strongly magnetised crust that holds clues to the planet's interior. The relation between magnetic anomalies and the underlying crustal magnetisation is complex because of magnetic structures that produce no observable field. We use a recently-developed method to isolate these "invisible" structures to explore explanations for the observations. The strong magnetisation suggested by ground observations from InSight can be obtained simply by adding a suitable invisible magnetisation to that required to explain the data. A thin Northern Hemisphere and thick Southern Hemisphere crust produces magnetic anomalies confined around the equator, not the Southern Hemisphere. Variations in crustal thickness produce differences with the satellite field, most notably strong anomalies associated with the impact craters that are not in the data. Magnetisation may be confined to depths greater than that of the craters, or anomalies from shallower material are not observable at satellite altitude.

Plain Language Summary

Four billion years ago Mars had a magnetic field generated by a dynamo operating in its liquid core, as Earth has today. It cooled faster than Earth and dynamo action ceased but not before it had magnetised the planet's crust. Their study is made topical by the arrival of the lander Perseverance and Chinese rover Zhurong, the latter capable of carrying out a ground magnetic survey . The lander InSight recorded a magnetic field some ten times stronger than expected from measurements made by satellite in orbit at altitude 150 km. Here we use a relatively new technique to separate proposed magnetic structures into their "invisible" and "visible" parts. We show this while the magnetic field is stronger in the Southern Hemisphere than the North, this does not imply one hemisphere is more strongly magnetised than the other. Strong ground measurements can be explained by a strongly magnetised, invisible, shell that has been broken up into smaller, visible, fragments. Larger impact craters have no magnetic anomaly, an observation often attributed to removal of the original magnetised material; we show the anomaly remains if the surrounding crust is strongly magnetised and propose the source of the anomalies lies deeper than the bottom of these craters.

1 Introduction

Determining magnetisation from observations of the crustal magnetic field is difficult because a wide variety of magnetised bodies do not have an observable field. This problem is particularly acute when the magnetisation is remanent, as on Mars, rather than induced, as on much of Earth's continents, because all 3 components of the vector magnetisation must be found rather than just the scalar susceptibility. Most interpretation is therefore done by forward modelling using a candidate distribution of magnetisation. Decomposition into vector spherical harmonics (VSH) separates the part of the magnetisation responsible for the observed field, the "visible" part, from the part that produces no magnetic field, the "invisible" part (Gubbins et al., 2011). This is useful because knowing the invisible part can direct further study using different data, such as gravity, geology, and topography. In this preliminary study we explore the value of VSH decomposition of models of Mars' crust.

Mars' remanent magnetisation has the same hemispheric dichotomy as the gravity field and topography: lowland plains in the Northern Hemisphere have weak magnetic fields whereas the mountains of the Southern Hemisphere have strong magnetic fields. The dichotomy is the oldest geology, thought to have formed when a dynamo was active in the core of Mars (Watters et al., 2007); younger geology with weaker magnetic fields is thought to have formed later, after the dynamo ceased to operate at around 4.1 Ga (Lillis et al., 2008), although some analyses put this date as late as 3.8 Ga (Hood et al., 2010).

The magnetic field has been measured by the orbiter Mars Global Surveyor and later by MAVEN in lower orbit, providing a global model with resolution around 150 km (Langlais et al., 2019). There is a single ground measurement, made by the lander InSight, which is some ten times that predicted by the orbital model (Johnson et al., 2020). There is a promise of further ground data in the near future from the NASA lander Perseverance and Chinese rover Zhurong, the latter carrying a magnetometer that could produce a small-scale survey.

Mars' crustal remanence is some ten times stronger than Earth's. It depends on the strength, morphology and timing of the primordial dynamo field, the magnetic minerals in the crust, and the thickness of the magnetised layer. Most studies start from a shell that becomes magnetised as the planet cooled early in its history, which is altered by subsequent activity [e.g. Milbury and Schubert (2010)]. Arkani-Hamed (2003, 2005) considered *secondary magnetisation* of a deeper layer that cooled below the Curie temperature after dynamo action ceased and was magnetised by the overlying magnetic layer. The depth of the magnetic layer is estimated at 30–65 km from spectra (Voorhies, 2008; Lewis & Simons, 2012), with an average of 50 km, close to the thickness of the crust estimated from gravity and topography (Wieczorek et al., 2019). Solomon et al. (2005) suggest the magnetic anomalies are associated with variations in crustal thickness.

The dichotomy is thought to have formed early in Mars' history by degree-1 mantle convection, which formed the northern plains and southern highlands (Zhong & Zuber, 2001; Nimmo & Gilmore, 2001; Ke & Solomatov, 2006), although an alternative theory invokes a giant impact or impacts hitting what is now the northern hemisphere (Frey & Schultz, 1988). Most authors have assumed a dipolar primordial dynamo field and there are many estimates of primordial paleopoles (Vervelidou et al., 2017). Stanley et al. (2008) explain the strong southern hemisphere magnetic fields with a hemispheric dynamo, which has magnetic field confined to one hemisphere. Degree-1 mantle convection would produce strong heat flux variations on the core-mantle boundary, inducing downwelling in the core. This concentrates magnetic field lines over the downwelling, a mechanism used to explain the concentration of Earth's magnetic field on the longitudes of the subduction zones of the Pacific rim (Bloxham & Gubbins, 1987).

The major magnetic features to be explained are the absence of anomalies in the northern lowlands, major impact basins of Hellas, Isidris, and Argyre, and part of the Tharsis bulge. These absences have been attributed to many different causes, including variation in crustal thickness, thermal demagnetisation, burial by later lavas erupted after dynamo action ceased, impact demagnetisation by excavation, and hydrothermal alteration (Solomon et al., 2005; Lillis et al., 2008, 2009; Morschhauser et al., 2018; Mittelholz et al., 2020). Thus a weak magnetic field region is normally taken to mean the crust beneath is weakly magnetised or thin, as in the northern lowlands; likewise, strong magnetic anomalies in the southern highlands are taken to mean strongly magnetised or thick crust. However, the relationship between magnetisation and magnetic field is not so simple: absence of magnetic field does not necessarily imply weak magnetisation.

In this preliminary survey use VSH decomposition to study 3 simple possible scenarios: a crust that is strongly magnetised everywhere, a new analysis of Arkani-Hamed's secondary magnetisation, and anomalies caused by a uniformly magnetised crust of variable thickness.

2 Method

VSH decomposition provides a generalisation of Runcorn's theorem (Runcorn, 1975), that a uniform shell magnetised by an internal dipole field produces no external field, used by Milbury and Schubert (2010) in their interpretation of Mars' magnetisation. The

VSH are simple combinations of scalar spherical harmonics

$$\boldsymbol{Y}^m_{n,n+1} = \frac{r^{n+2}}{\sqrt{(n+1)(2n+1)}}\nabla\left[\frac{1}{r^{n+1}}Y^m_l(\theta,\phi)\right] \quad (1)$$

$$\boldsymbol{Y}^m_{n,n} = -\frac{i}{\sqrt{n(n+1)}}\boldsymbol{r}\times\nabla Y^m_n(\theta,\phi) \quad (2)$$

$$\boldsymbol{Y}^m_{n,n-1} = \frac{1}{r^{n-1}\sqrt{n(2n+1)}}\nabla\left[r^n Y^m_n(\theta,\phi)\right]. \quad (3)$$

where Y^m_n is a complex mean-normalised scalar spherical harmonic. They are complete and orthogonal when integrated over the sphere. The appearance of r in (1)–(3) is illusory because it differentiates out. The VSH are written in this way to bring out the connection with the 3 types of solution of Laplace's equation: the potential field finite at infinity, $\boldsymbol{Y}^m_{n,n+1}$, the one finite at the origin, $\boldsymbol{Y}^m_{n,n-1}$, and the toroidal one, $\boldsymbol{Y}^m_{n,n}$, that has an associated radial electric current. An immediate consequence is that a uniform shell magnetised by an internal magnetic field will contain only $\boldsymbol{Y}^m_{n,n-1}$ harmonics; likewise magnetisation by an external magnetic field will contain only $\boldsymbol{Y}^m_{n,n+1}$ harmonics.

In this paper we deal only with the vertically integrated magnetisation (VIM) and assume magnetisation is confined to a surface shell that is thin compared to the radius of the planet. We expand the VIM in VSH:

$$\bar{\boldsymbol{M}}(r,\theta,\phi) = \sum_{n,m} E^m_l\boldsymbol{Y}^m_{n,n+1}(\theta,\phi) + I^m_n\boldsymbol{Y}^m_{n,n-1}(\theta,\phi) + T^m_n\boldsymbol{Y}^m_{n,n}(\theta,\phi) = \mathcal{E}+\mathcal{I}+\mathcal{T}. \quad (4)$$

The coefficients are integrals of the magnetisation; orthogonality gives

$$E^m_n = \frac{1}{4\pi}\oint \bar{\boldsymbol{M}}\cdot(\boldsymbol{Y}^m_{n,n+1})^* d\Omega \quad (5)$$

$$I^m_n = \frac{1}{4\pi}\oint \bar{\boldsymbol{M}}\cdot(\boldsymbol{Y}^m_{n,n-1})^* d\Omega \quad (6)$$

$$T^m_n = \frac{1}{4\pi}\oint \bar{\boldsymbol{M}}\cdot(\boldsymbol{Y}^m_{n,n})^* d\Omega, \quad (7)$$

where $*$ denotes the complex conjugate.

The associated magnetic fields in the non-magnetic, insulating external and internal regions are found by substituting into the usual Poisson integral. This shows that the $\{\boldsymbol{Y}^m_{n,n-1}\}$ produce a potential outside the sphere but none inside it, the $\{\boldsymbol{Y}^m_{n,n+1}\}$ inside the sphere but none outside it, and the $\{\boldsymbol{Y}^m_{n,n}\}$ no potential field at all because the associated radial electric current cannot flow in the insulator.

The $\boldsymbol{Y}^m_{n,n-1}$ coefficients, $\{I^m_n\}$, are related to the usual Gauss coefficients:

$$g^m_n = \frac{\mu_0}{r_{\rm E}}\sqrt{n\epsilon_m}\,\Re(I^m_n) \quad (8)$$

$$h^m_n = -\frac{\mu_0}{r_{\rm E}}\sqrt{n\epsilon_m}\,\Im(I^m_n), \quad (9)$$

where

$$\epsilon_m = 2-\delta_{m0}. \quad (10)$$

The I^m_n therefore describe the visible part of the magnetisation, the E^m_n and T^m_n the invisible part. They form the complete null space of the inverse problem of magnetisation from magnetic field data.

Runcorn's theorem follows immediately: an internal dipole magnetising a uniform shell involves only E^0_1 and is therefore invisible. However, the full set of invisible structures includes all $\mathcal{E}$ and $\mathcal{T}$ terms. The $\mathcal{E}$ part includes magnetisation of a uniform shell by any internal field, not just a dipole. In particular the hemispheric dynamo proposed

by Stanley et al. (2008) will not produce a magnetic dichotomy on its own, a non-uniform crust or external field is also needed. Importantly for Mars, a uniform shell will produce an external field if it is deformed, for example by faulting, erosion, or mineral alteration. Even removal of magnetic material by thermal demagnetisation, erosion, or impact will produce a magnetic signal rather than removing one.

Full details of the method are given in Gubbins et al. (2011).

3 A Uniform Shell With Secondary Magnetisation

3.1 Strong VIM beneath weak magnetic anomalies

The simplest model of Mars' early magnetic crust is a uniform shell cooling from above and magnetised by an internal dynamo-generated field $\boldsymbol{B}$. The VIM is

$$\bar{\boldsymbol{M}} = \Xi d\boldsymbol{B}/\mu_0, \tag{11}$$

where d is the thickness of the magnetised layer and the magnetising constant $\Xi = K\chi/(1+\chi)$ can be estimated from the Koenigsberger ratio K and susceptibility χ. For an internal dipole magnetising field the E coefficients are simply related to the $n = 1$ Gauss coefficients: $E_1^0 = -\sqrt{2}\Xi d/\mu_0 g_1^0$ and $E_1^1 = -\Xi d/\mu_0(g_1^1 - ih_1^1)$. The strength of VIM is determined by a single scalar, the product of the dipole moment and Ξd, which can be adjusted within reasonable bounds to fit any required observation.

This basic VIM must be altered if it is to fit the present-day data. To do this we add an $\mathcal{I}$ component based on the Gauss coefficients of Langlais et al. (2019) using equations (8) and (9). The resulting VIM fits the data exactly and contains an arbitrarily strong background magnetisation. Although the uniform shell does not produce any external magnetic field it does change the orientation and strength of the VIM locally. In particular it affects the VIM at landing sites and, if the shell has undergone subsequent alteration, will partly determine the magnetic anomalies at the planet's surface.

Three examples of the radial component of VIM are shown in Figure 1 for 3 dipole orientations, axial, equatorial and one taken from previous estimates of Mars' paleopole (Milbury & Schubert, 2010). We have chosen $K = 1,\ \chi = 0.2,\ d = 40$ km, and $G = \sqrt{g_1^{02} + g_1^{12} + h_1^{12}} = 30,000$ nT: reasonable values for magnetic minerals, a commonly quoted thickness for Mars' magnetised crust [e.g. Voorhies (2008)], and an Earth-like dipole field. These choices make the strength of magnetisation of the uniform shell comparable with that required to satisfy the magnetic field model. In Table 1 we give the magnetic vectors at 3 sites on Mars, the landing sites of InSight, Perseverance, and Zhurong. The differences in magnetic vectors caused by the uniform shell and different dipole orientations is clear.

3.2 Secondary Magnetism

Arkani-Hamed (2003) considered cooling of Mars' crust beyond the duration dynamo action, giving 2 shells, the upper one magnetised by the dynamo and the lower one by the magnetic field of the upper one. Suppose for simplicity the outer shell, thickness d_u, was magnetised by an axial dipole; its VIM is described by the single VSH coefficient $E_1^0 = \sqrt{2}\Xi d_\mathrm{u}/\mu_0 g_1^0$, which produces a field inside the shell with Gauss coefficient

$$r_1^0 = \sqrt{2}\mu_0 E_1^0/R_{\male} = 2\Xi g_1^0 d_\mathrm{u}/R_{\male},$$

where $R_{\male}$ is Mars' radius. The internal shell, now grown by continued cooling to a thickness d_l, is magnetised by the external field with VIM described by a single VSH coefficient $I_1^0 = \Xi d_\mathrm{l}/\mu_0 r_1^0 = 2\Xi^2 d_\mathrm{u} d_\mathrm{l}/\mu_0 R_{\male}$. The secondary magnetisation of the inner shell, unlike the outer shell, does produce an external field with Gauss coefficient

$$j_1^0 = \mu_0 I_1^0/R_{\male} = 2\Xi^2 (d_\mathrm{u}/R_{\male})(d_\mathrm{l}/R_{\male}) g_1^0. \tag{12}$$

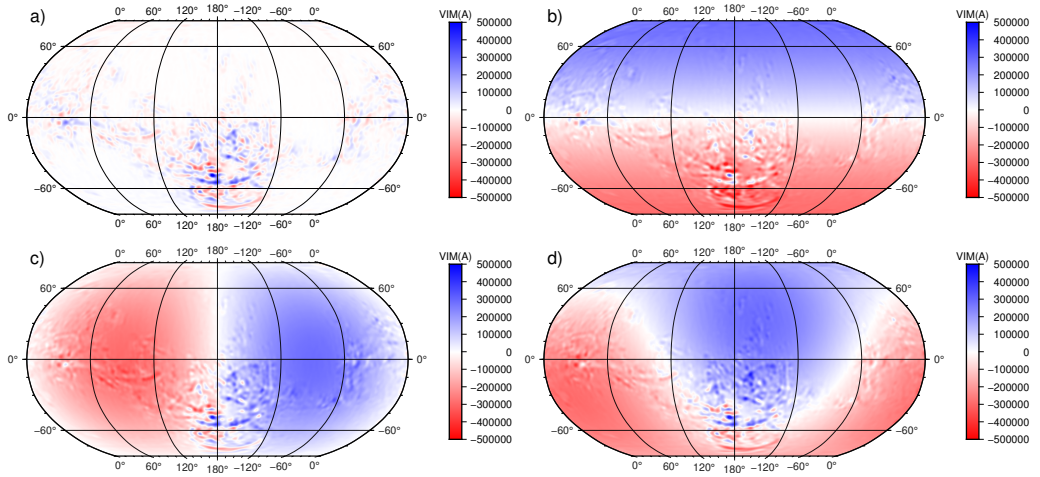

Figure 1. Radial components of VIM by different dipoles. a: $\mathcal{I}$ "visible" part based on the satellite field using (8) and (9); b: addition of a uniform shell magnetised by an internal axial dipole; c: same for an equatorial dipole with paleopole 0°N,270°E; d: for a dipole with paleopole 34°N,202°E.

Lander	InSight			Perseverance			Zhurong		
	Mag	Dip	Az	Mag	Dip	Az	Mag	Dip	Az
B nT	309.91	-73°	135°	90.84	-64°	134°	80.65	47°	55°
M(I) kA	17.2	-57°	-61°	3.01	5°	-147°	5.78	55°	-157°
M(axi) kA	159	-14°	-177°	183	-33°	-179°	195	-41°	0.03°
M(equ) kA	241	60°	-92°	301	78°	148°	289	73°	-140°
M(gen) kA	229	51°	-128°	193	59°	167°	204	51°	-160°

Table 1. Magnetic fields and magnetisations at the sites of the 3 landers on Mars. Their locations are: InSight (4.5°N,135.6°E), Perseverance (18.4°N,77.5°E), Zhurong (25.1°N,109.9°E). B denotes the magnetic field computed from the satellite model of Langlais et al. (2019). M(I) the vector VIM in Amps computed by converting the Gauss coefficients of the satellite model to I_n^m using equations (8) and (9). The last 3 lines are VIMs after addition of a uniform shell magnetised by a dipolar dynamo field with axial, equatorial, and general paleopoles as described in the text. Note the dominance of the magnetisation of the uniform shell, an order of magnitude larger than the $\mathcal{I}$ part. This is because of the dominance of the $\mathcal{E}$ part from magnetisation by an internal field. The same applies to the Earth (Masterton et al., 2012).

This external field is a reflection of the primordial dynamo field reduced by the factor $\Xi^2(d_u/R_{\sigma'})(d_l/R_{\sigma'})$. Taking the previous value for g_1^0, Ξ and $d_u = d_l = 20$ km gives $j_1^0 \approx 1$ nT, the same order of magnitude as the Langlais et al. (2019) model but much smaller than the high degree terms. The similarity in orders of magnitude make secondary magnetisation an interesting possible contributor but, in agreement with Arkani-Hamed (2005), we find it too small to explain the small-scale anomalies.

The same analysis applies to any dynamo field, whether off-axis dipole or multipolar, such as a hemispheric field. In future, if the crustal structure can be tied down sufficiently accurately, secondary magnetisation offers an interesting window on Mars' original dynamo field.

4 A Magnetised Shell of Variable Thickness

We now explore to what extent the magnetic anomalies can be explained by variable crustal thickness. The hemispheric dichotomy suggests a thin layer in the Northern Hemisphere and a thick layer in the Southern Hemisphere. The resulting magnetisation by any primordial field is a substantial $\mathcal{E}$ part resulting from a uniform layer with Northern Hemisphere thickness plus an extra Southern Hemisphere layer also dominated by $\mathcal{E}$ except on the boundary because it is uniform within the hemisphere. The resulting magnetic field is concentrated around the equator irrespective of the primordial magnetising field. More details are in the Supplementary Information, see Figures S1-3.

We next assume a crust with uniform magnetic properties but variable thickness $d(\theta, \phi)$ derived from topography and gravity using the methods described in Wieczorek et al. (2019). Figure 2 shows the initial thickness assuming a uniform crustal density 2.9 kg/cm^3, mantle density 3.4 kg/cm^3, imposed 40 km thickness at the InSight landing site, and maximum spherical harmonic degree 90. The VIM is, from (11), $\bar{\boldsymbol{M}}(\theta, \phi) = (\Xi d(\theta, \phi)/\mu_0)\boldsymbol{B}(\theta, \phi)$ with $K = 3$, $\chi = 0.5$ and $G = -30,000$ nT. We use the same 3 primordial paleopoles

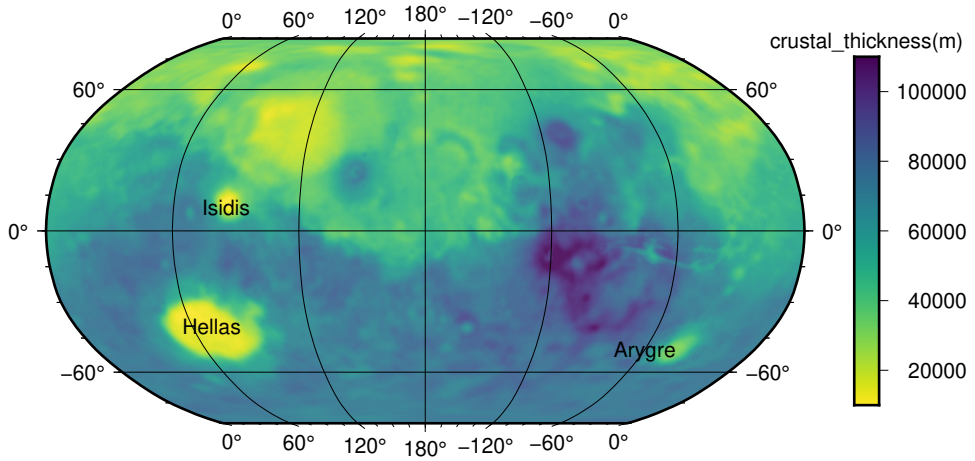

Figure 2. Crustal thickness for Mars based on inversion of topography and gravity data (Wieczorek et al., 2019).

as before.

Each VIM is decomposed into VSH as illustrated in Figure 3. Only the radial component is shown, for which the toroidal component is zero. Note that the $\mathcal{E}$ part on the left reflects the dipole orientation and some of the variations in crustal thickness, most noticeably the Hellas basin; it is some 10 times larger than $\mathcal{I}$, as is the case for Earth (Masterton et al., 2012). The relative sizes (RMS) of the total VIMs are $\mathcal{E} : \mathcal{T} : \mathcal{I} =$ 81:9:10. $\mathcal{E}$ dominates because the crustal thickness is to a first approximation a uniform shell and it is magnetised by an internal field. The $\mathcal{I}$ part is mainly determined by variations in crustal thickness rather than dipole orientation.

Radial magnetic fields are shown in Figure 4. Like the $\mathcal{I}$ part, the field patterns are relatively insensitive to dipole orientation.

The wavelengths are similar to the satellite model but there are large discrepancies, most noticeably the anomalies over major impact craters Hellas, Isidis, and Argyre. The crustal models all produce crater anomalies that are wholly absent from the satellite model. Hellas has the largest anomaly; it lies in a region of thick (>60 km) crust and has a sharp step around its edge that produces the more intense ring on the boundary

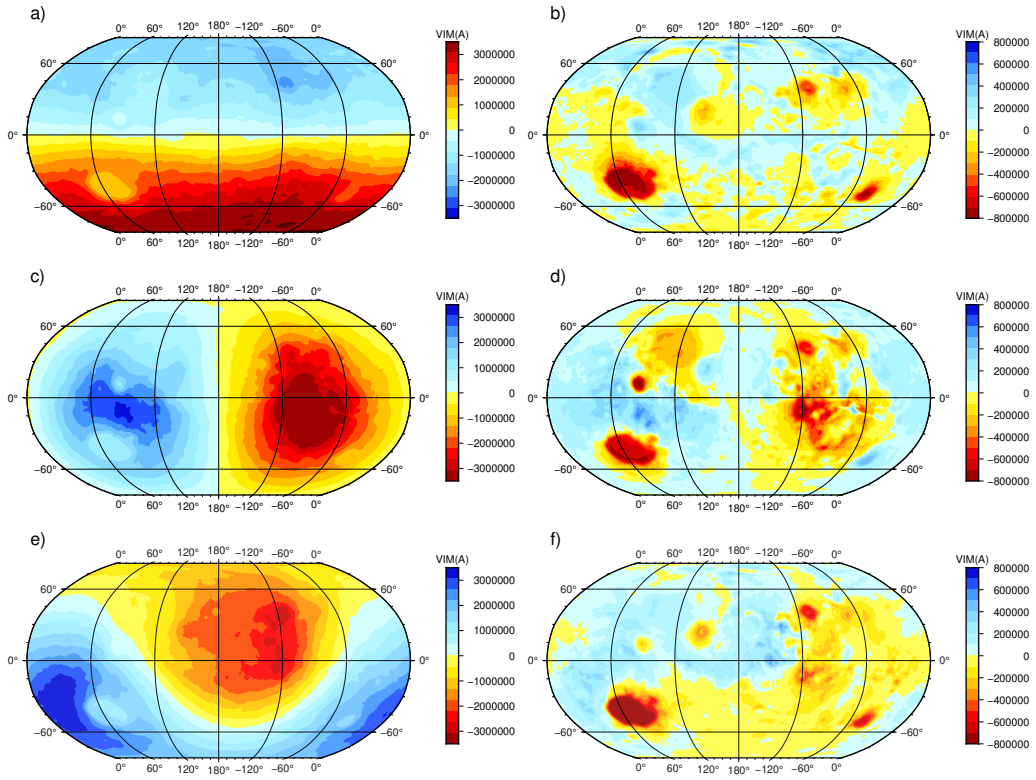

Figure 3. VSH decomposition of the radial component of VIM for 3 paleopoles. Columns are $\mathcal{E}$ (left) and $\mathcal{I}$ (right); rows are for axial, equatorial (0°N,270°E), and general (34°N,202°E) paleopoles. Radial component for $\mathcal{T}$ is zero.

(Figures 4, 5). Isidis lies in a region of thinner crust and the anomaly is not so prominent (Figure(S5)). Magnetic anomalies are more subdued or absent along more gradual gradients in crustal thickness such as the dichotomy boundary and the margins of Utopia Planitia. This suggests the sharp jumps in VIM near the periphery of the boundaries are responsible for at least part of the anomalies. Absence of crater anomalies has been addressed by Lillis et al. (2010), who favour impact demagnetisation. Their models invoked a magnetic layer with uniform thickness but spatially varying magnetic properties that give rise to sizeable magnetic anomalies. By completely removing magnetisation within an inner circle, and allowing the magnetisation to 'ramp up' within an annulus around this circle, they reduced the predicted anomalies. We change the thickness of the magnetised layer in a similar way, which should have the same effect on the VIM as changing the magnetisation. Our models differ in that they do not consider any spatial variations in crustal magnetic properties.

We removed the sharp step in VIM around Hellas by replacing the original thickness values in an annular region with radii 500km and 2000km, centered on the middle of the crater, with values derived by minimum curvature interpolation of the thickness outside the annulus as shown in Figure 5e. The magnetic anomaly is reduced (Figure 5c but still substantial. We then returned to our central thesis, that a uniform VIM produces no magnetic anomaly, and interpolated across the entire crater, essentially filling it in. This does remove the magnetic anomaly (Figure 5d), but is hard to justify physically. One possible explanation is that the magnetic layer lies deep within the crust and any removal of shallow, non-magnetic material makes no difference. The problem is discussed further in Section 5.

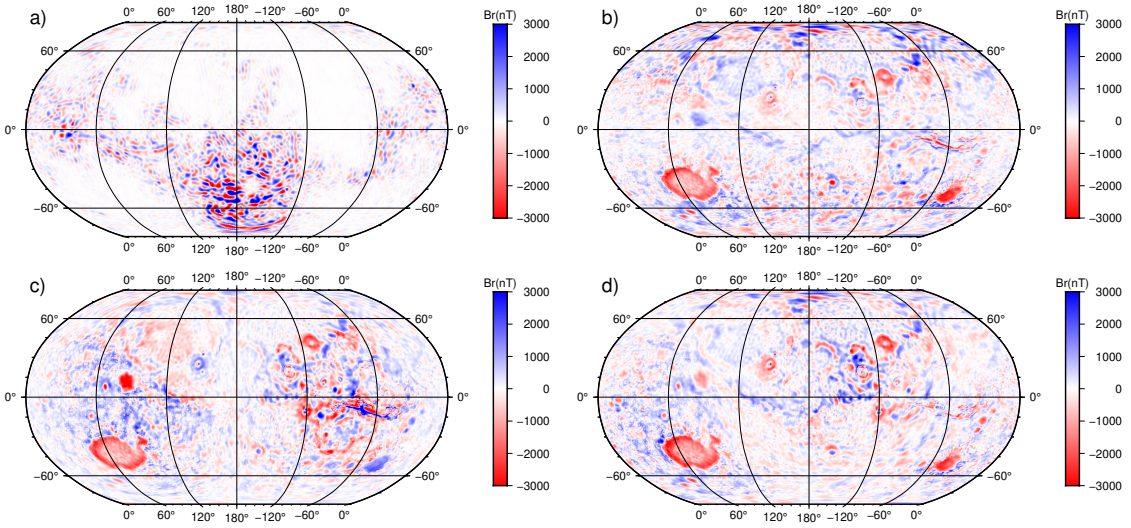

Figure 4. Radial component of the magnetic field at Mars surface. a: Satellite model (Langlais et al., 2019); b: from VIM proportional to crustal thickness, magnetising field axial dipole ; c: equatorial dipole (0°N,270°E); d: general paleopole (34°N,202°E).

Results for the other 2 craters, Isidis and Argyre, are shown in Figure S6, S7.

VSH decomposition of the VIM for each of the 3 crustal thickness models shows that the $\mathcal{E}$ component is reduced at the expense of $\mathcal{I}$ and $\mathcal{T}$ by interpolation but is increased by filling in. The RMS ratios $\mathcal{E}$:$\mathcal{I}$:$\mathcal{T}$ are 81:10:9, 81:10:9 and 85:7:8 respectively. This is to be expected as interpolation removes a small part of the shell whose magnetism is dominated by the $\mathcal{E}$ part (but not enough to change the ratios at this resolution) while filling in adds material that is dominated by the $\mathcal{E}$ part.

Similar results and conclusions apply to the other craters, Isidis and Argyre, see the Supplementary Information Figures S6, S7.

5 Discussion and Conclusions

We have explored the use of VSH decomposition in evaluating possible magnetisation structures that could produce the observed Martian magnetic field. The ground measurement by InSight proves the existence of strong anomalies with wavelengths too short to be seen at satellite altitude. This requires strongly magnetised material at a relatively flat site that would not normally be thought as highly magnetic. Johnson et al. (2020) use Parker's ideal body theory to estimate a lower bound on the magnetisation. They assume 40 km-thick magnetised layers starting at depths from 200 m down to 10 km and require magnetisations of 1.4–24 Am^{-1} or VIM $0.56-9.60\times10^5$ A, similar to the RMS of our $\mathcal{I}$ part of 2.3 10^5 A. This is below the value required to explain the strong Southern Hemisphere anomalies (Johnson et al., 2020). However, we find an additional invisible $\mathcal{E}$ part some 10 times larger. The true magnetisation and/or layer thickness is therefore likely to be much larger than anything envisaged so far.

Arkani-Hamed's inner shell of secondary magnetisation is interesting because, unlike the primary magnetisation, it is capable of producing an observable magnetic field. The VSH decomposition provides an exceptionally simple demonstration of this. While we have little new to report beyond that already published, VSH gives an elegant and simple formalism for exploring the primordial magnetising field.

Changing the primordial field from a dipole to a more complicated structure, such as a hemispheric one, does not produce anomalies without an appropriate distribution of VIM. The simplest model, a thin magnetised layer in the northern hemisphere and a thick one in the south, only produces magnetic anomalies around the equator because of the uniform magnetisation elsewhere: more complex structures are essential.

The next simplest layer is one with uniform magnetisation but variable thickness. We take the crustal thickness derived from gravity and topography and compare the resulting magnetic field with observations. The model is too simple to justify any detailed comparison but there is a glaring disparity around the major impact craters, notably Hellas. The absence of magnetic anomalies above the craters cannot be explained by simply excavating magnetised material by an impact after dynamo action ceased because strong anomalies would be created by the sharp crater rims. Smoothing out these edges reduces the anomalies somewhat but still fails to match observations. Filling in the craters eliminates the anomaly altogether, as required. This could mean that the large scale anomalies observed at satellite altitude are dominated by deep magnetic structures, deeper than the bottom of the craters, with the surface layers fractured to such an extent that they only produce anomalies with scales less than 150 km that do not show up at satellite altitude.

Our long term goal is to develop a geologically plausible model for the magnetised layer at Mars' surface; one based on the crustal thickness may be a starting point. Our aim will be helped by future ground measurements from NASA's lander Perseverance and the Chinese rover Zhurong.

Acknowledgments

KZ is supported by the Macau Science and Technology Development Fund, grant No. 0005/2019/A1 and by the Pre-research Project on Civil Aerospace Technologies No. D020303 funded by China National Space Administration. SW is supported by NSFC project 41972237. YJ is supported by Macau Foundation. Our analysis made use of the codes ctplanet and pyshtools (Wieczorek & Meschede, 2018).

References

Arkani-Hamed, J. (2003). Thermoremanent magnetisation of the Martian lithosphere. *J. Geophys. Res.*, *108*, 5114. doi: 10.1029/2003JE00204

Arkani-Hamed, J. (2005). Magnetic crust of Mars. *J. Geophys. Res.*, *110*(E8), 20p. doi: 10.1029/2004JE002397

Bloxham, J., & Gubbins, D. (1987). Thermal core-mantle interactions. *Nature*, *325*, 511–513.

Frey, H., & Schultz, R. (1988). Large impact basins and the mega-impact origin for the crustal dichotomy on Mars. *Geophys. Res. Lett.*, *15*(3), 229–232.

Gubbins, D., Ivers, D., Masterton, S. M., & Winch, D. E. (2011). Analysis of lithospheric magnetisation in vector spherical harmonics. *Geophys. J. Int.*, *187*, 99–117.

Hood, L. L., Harrison, K. P., Langlais, B., Lillis, R. J., Poulet, F., & Williams, D. A. (2010). Magnetic anomalies near Apollinaris Patera and the Medusae Fossae Formation in Lucus Planum, Mars. *ICARUS*, *208*(1), 118–131.

Johnson, C. L., Mittelholz, A., Langlais, B., Russell, C. T., Ansan, V. x. r., Banfield, D., ... Banerdt, W. B. (2020). Crustal and time-varying magnetic fields at the InSight landing site on Mars. *Nature Geoscience*, *13*(3), 1–13.

Ke, Y., & Solomatov, V. S. (2006). Early transient superplumes and the origin of the Martian crustal dichotomy. *J. Geophys. Res.*, *111*, E1001. doi: 10.1029/2005JE002631

Langlais, B., Thébault, E., Houliez, A., Purucker, M. E., & Lillis, R. J. (2019). A

New Model of the Crustal Magnetic Field of Mars Using MGS and MAVEN. *J. Geophys. Res.-Planets*, *124*(6), 1542–1569.

Lewis, K. W., & Simons, F. J. (2012). Local spectral variability and the origin of the Martian crustal magnetic field. *Geophys. Res. Lett.*, *39*(18), 790. doi: 10.1029/2012GL052708

Lillis, R. J., Dufek, J., Bleacher, J. E., & Manga, M. (2009). Demagnetization of crust by magmatic intrusion near the Arsia Mons volcano: Magnetic and thermal implications for the development of the Tharsis province, Mars. *J. Volcanology Geothermal Res.*, *185*(1-2), 123–138.

Lillis, R. J., Frey, H. V., & Manga, M. (2008). Rapid decrease in Martian crustal magnetization in the Noachian era: Implications for the dynamo and climate of early Mars. *Geophys. Res. Lett.*, *35*(14). doi: 10.1029/2008GL034338

Lillis, R. J., Purucker, M. E., Halekas, J. S., Louzada, K. L., Stewart-Mukhopadhyay, S. T., Manga, M., & Frey, H. V. (2010). Study of impact demagnetization at Mars using Monte Carlo modeling and multiple altitude data. *J. Geophys. Res. E: Planets*, *115*(7). doi: 10.1029/2009JE003556

Masterton, S., Gubbins, D., Mueller, D., Ivers, D., & Hemant, K. (2012). Forward modelling of oceanic lithospheric magnetisation. *Geophys. J. Int.*, *192*, 951–962.

Milbury, C., & Schubert, G. (2010). Search for the global signature of the Martian dynamo. *J. of Geophys. Res.*, *115*(E10), 790–15.

Mittelholz, A., Johnson, C. L., Feinberg, J. M., Langlais, B., & Phillips, R. J. (2020). Timing of the martian dynamo: New constraints for a core field 4.5 and 3.7 Ga ago. *Science Advances*, *6*(18), eaba0513.

Morschhauser, A., Vervelidou, F., Thomas, P., Grott, M., Lesur, V., & Gilder, S. A. (2018). Mars' Crustal Magnetic Field. In *Magnetic fields in the solar system* (pp. 331–356). Springer International Publishing.

Nimmo, F., & Gilmore, M. (2001). Constraints on the depth of magnetized crust on Mars from impact craters. *J. Geophys. Res.*, *106*, 12,315–12,323.

Runcorn, S. K. (1975). On the interpretation of lunar magnetism. *Phys. Earth Planet. Int.*, *10*, 327–335.

Solomon, S. C., Aharonson, O., Aurnou, J. M., Banerdt, W. B., Carr, M. H., Dombard, A. J., ... Zuber, M. T. (2005). New Perspectives on Ancient Mars. *Science*, *307*(5713), 1214–1220.

Stanley, S., Elkins-Tanton, L., Zuber, M. T., & Parmentier, E. M. (2008). Mars' Paleomagnetic Field as the Result of a Single-Hemisphere Dynamo. *Science*, *321*(5897), 1822–1825.

Vervelidou, F., Lesur, V., Morschhauser, A., Grott, M., & Thomas, P. (2017). On the accuracy of palaeopole estimations from magnetic field measurements. *Geophys. J. Int.*, *211*(3), 1669–1678.

Voorhies, C. V. (2008). Thickness of the magnetic crust of Mars. *J. Geophys. Res.-Planets*, *113*(E04004). doi: 10.1029/2007JE002928

Watters, T. R., McGovern, P. J., & Irwin III, R. P. (2007). Hemispheres Apart: The Crustal Dichotomy on Mars. *Ann. Rev. Earth Plan. Sci.*, *35*(1), 621–652.

Wieczorek, M. A., Beuthe, M., Rivoldini, A., & Van Hoolst, T. (2019). Hydrostatic Interfaces in Bodies With Nonhydrostatic Lithospheres. *J. Geophys. Res.-Planets*, *124*(5), 1410–1432.

Wieczorek, M. A., & Meschede, M. (2018). SHTools: Tools for Working with Spherical Harmonics. *Geochem., Geophys., Geosys.*, *19*, 2574–2592.

Zhong, S., & Zuber, M. (2001). Degree-1 mantle convection and the crustal dichotomy on Mars. *Earth Planet. Sci. Lett.*, *189*, 75–84.

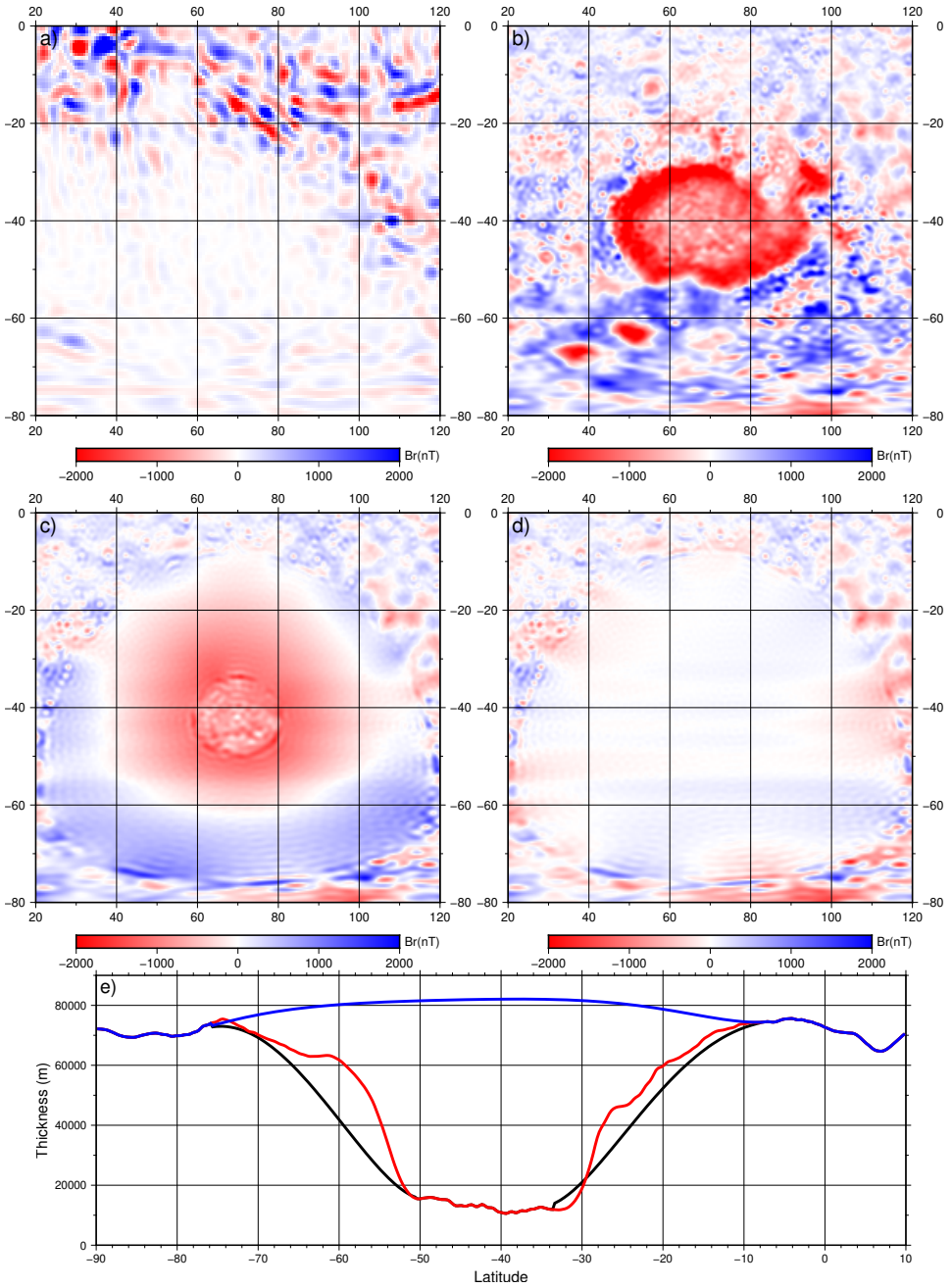

Figure 5. Close-up of the Hellas anomaly illustrating radial component of the magnetic field. a: Satellite model (Langlais et al., 2019); b: original crustal thickness model; c: model with steep crater shoulders from (b) replaced with minimum curvature interpolation; d: crater removed altogether. e: North-South profile extracted along Longitude 70°E showing the crustal thickness profiles for the model cases shown in b (red), c (black) and d (blue) respectively.